HYBRID SOFT SOIL TIRE MODEL (HSSTM).

PART III: MODEL PARAMETERIZATION AND VALIDATION

Sandu, C.[a,1] , Taheri, Sh.[b] , Taheri, S.[a], Els, S.[c], Jimenez, E. [d]

[a]*Department of Mechanical Engineering, Virginia Tech, Blacksburg, VA, USA*

[b]*Pratt and Miller, NC, USA*

[c]*Department of Mechanical Engineering, University of Pretoria, Pretoria, South Africa*

[d]*Navistar, Chicago, IL, USA*

Highlights

- HSSTM parameterization via standard measurements, modal analysis, and FEM is presented.
- Modal analysis includes set-up, quasi-static loading test, and estimating tire modal shapes.
- Theoretical in-plane vibration analysis and parameter estimation procedure are presented.
- Validation results are presented for the simulation results of HSSTM against tests performed in the Terramechanics test rig.

Abstract

Part I describes the tire structure model; part II the contact detection and contact interface models for rigid and deformable terrains; part III the model parameterization and validation. Model parameters are estimated using non-linear least-square optimization to minimize the error between the Hybrid Soft Soil Tire Model (HSSTM) predictions and experimental data. The parameterization routines' initial conditions are estimated from modal analysis in radial and circumferential directions. The preliminary parameterized model is incorporated in the optimization routine to find tire sidewall and belt parameters in the radial direction using quasi-static cleat loading test data. The vertical force at the spindle and tire contact patch are used to study the model accuracy in the radial direction. FlatTrac tire longitudinal and lateral force test data are employed to estimate the parameters in these directions. The tire shear force and moment at the spindle are validated against experimental data for lateral dynamics performance.

Keywords: HSSTM; Tire Model; Least-square Optimization, Parameterization; Modal Analysis

[1] Corresponding author email address: csandu@vt.edu

1. Introduction

The Hybrid Soft Soil Tire Model (HSSTM) was developed in order to efficiently estimate tire forces and moments with higher fidelity than other semi-analytical tire models, on rigid as well as on deformable terrain. The implementation of the tire structure model was described in [1]. Furthermore, the modeling of the tire-terrain interaction was elaborated in [2]. The HSSTM parameter estimation practices are presented in this study. The tire model parameter estimation is defined as the set of experiments and data processing methods that are performed to parameterize the tire model. There are different methods that can be used for tire model parameter estimation. These methods range from completely empirical to semi-empirical methods. For the model developed in this study, a complete set of tire parameterization methods for individual parameters is proposed. In Figure 1, the types of parameters that can be obtained from each set of tests are shown.

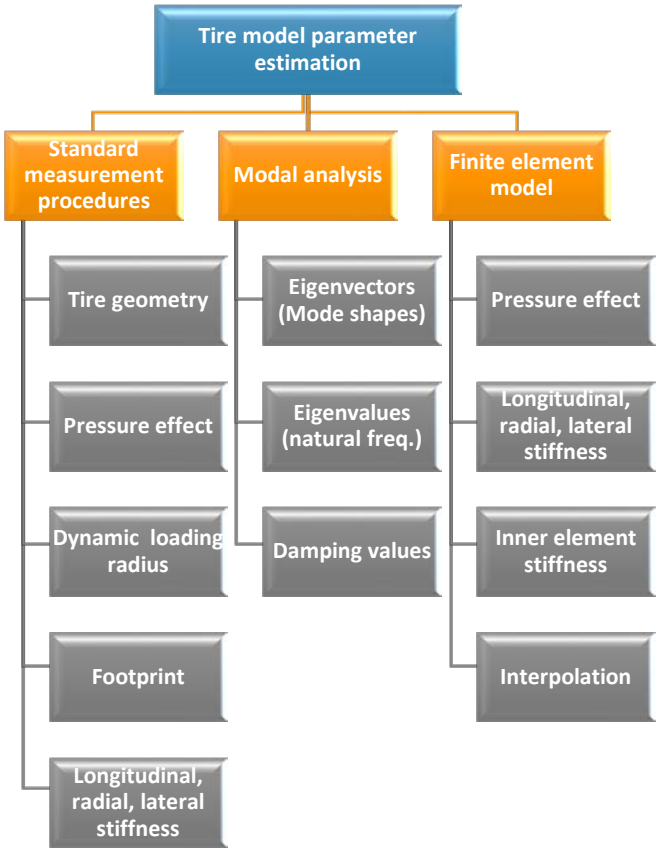

Figure 1: Tire model parameter estimation procedures used for defining the tire model parameters, and tire parameters resulted from post-processing of each set of tests.

For the HSSTM, the stiffness and the damping characteristics of the tire are considered to be different for in-plane and out-of-plane directions. As a result, during the loading of the tire in the vertical direction, for example, the

slope of the tangent line to the load-deflection curve is not just due to the in-plane radial stiffness of the tire. It is not always effective to rely solely on standard measurement procedures in order to measure stiffness and damping parameters. Furthermore, conducting a wide variety of tests on the tire in different configurations, such as axial and tangential loading, tire relaxation time measurements, and cleat tests requires a large amount of time and resources, which may not always be feasible.

Having these limitations in mind, a finite element model (FEM) of the tire has been implemented [3, 4], which can be used for simulating virtual parameterization tests, as well as for the validation of the lumped mass soft-soil tire model simulations. The tire tread is not considered in the initial version of the FEM model to simplify the validation of the lumped mass tire model. Some material properties of the FEM model were obtained from the manufacturer documentation; the rest of the required properties were obtained through experimental tests done on a similar tire by other researchers [5]. The FEM model validation based on Tire Model Performance Test (TMPT) data is done qualitatively and quantitatively. The details of the TMPT program are explained in the "Experimental study" section. In the qualitative method, the trend of the data with different parameter changes is studied. The quantitative approach compares measured data from two similar simulations done with different methods. The tire FEM model used in this study is developed by the author and presented in his M.S. thesis [3]. The tire FEM is initially compared with steady-state experimental data.

An optimization routine is developed to estimate a set of model parameters that can result in the highest correlation between the model estimations and the test data. The overview of the parameterization procedure is shown in Figure 2. The nonlinear curve-fitting procedure is implemented as a least-squares optimization [6]. The cost function for this optimization problem reads:

$$\min_{\lambda} \|\Omega(\lambda, inputs) - responses\|_2^2 = \min_{\lambda} \sum_i \left(\Omega(\lambda, input_i)\right)^2 \quad (1)$$

Where Ω is the tire structure model outputs, *responses* are corresponding system output from the test data, and λ is the set of model parameters. Having a correct estimation of the tire model parameters as the initial conditions in the optimization algorithm is crucial in its fast convergence to the final set of model parameters that can minimize the cost function [7]. The "lsqcurvefit" function in MATLAB is used to solve the optimization problem. The function solver is set to the trust-region-reflective algorithm [8]. This algorithm is a subspace trust-region method

and is based on the interior-reflective Newton method [9]. Each iteration involves the approximate solution of a large linear system using the method of preconditioned conjugate gradients (PCG).

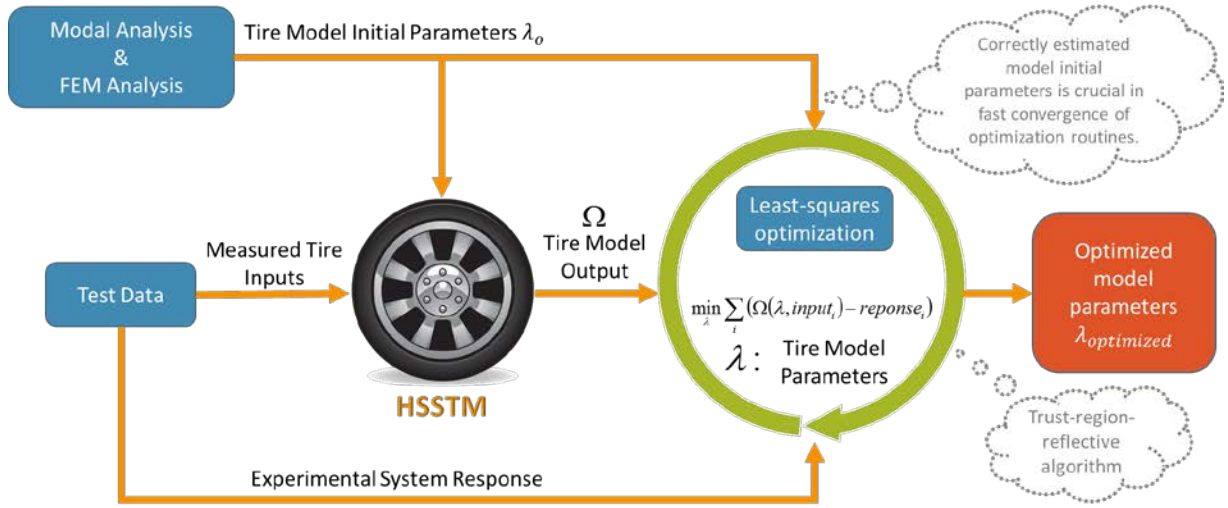

Figure 2: Overview of the HSSTM parameter estimation procedure

The parameters for tire materials models were identified using two different approaches. The in-plane stiffness and damping values were calculated using modal analysis tests and plate loading. The out-of-plane stiffness and damping values were estimated using the flat track machine data, as well as virtual tests conducted with a validated FEM tire model [3,4]. The experimental setups are described in more details in the following chapters.

1. Modal Analysis Test Setup

The modal analysis test was performed in order to extract tire mode shapes and associated natural frequency and damping values. These values were directly used for the parameterization of the HSSTM. The schematic of a test rig typically used for conducting radial modal analysis experiments on tires is illustrated in Figure 3. The tire is hanged from a steel structure by cords to avoid the effect of the mounting structure on the vibrational characteristics of the tire. Tri-axial accelerometers are attached at ten equally spaced locations on the tire surface with heated beeswax. The accelerometers used are very small, so they would not change the structural characteristics of the tire at the installation location.

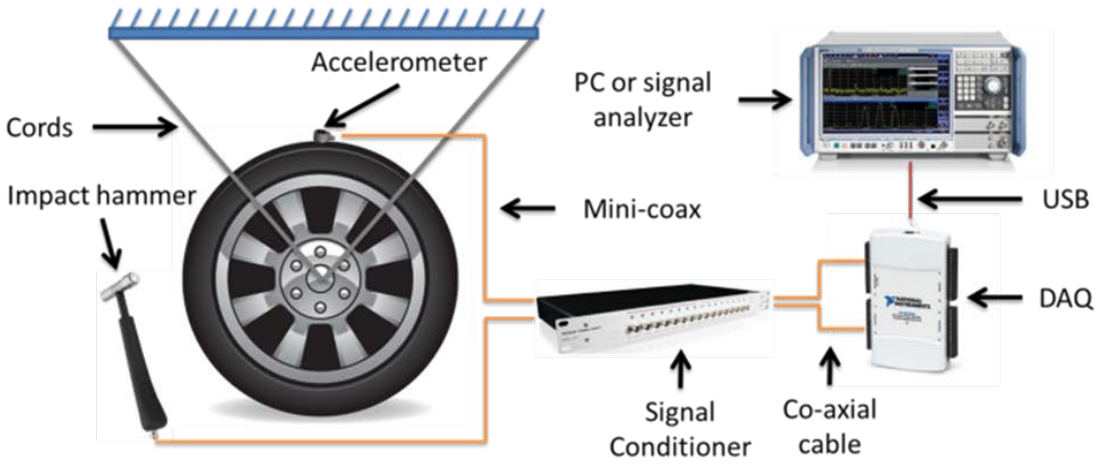

Figure 3: The modal analysis test rig schematic for extracting the tire natural frequencies and damping values. These values are used accordingly to parameterize the tire material model.

The tire is excited with an impulse force generated by an instrumented handheld hammer. In order to achieve accurate estimations for the frequency response functions, the input energy to the tire should be uniformly distributed over the frequency range of interest. To achieve this ideal input excitations, a plastic material is used as the tip of the hammer, and a piece of aluminum is mounted on the tire at the impact location. The signals from the hammer force transducer and accelerometers are amplified by a signal conditioner to reach the voltage levels that can be detected by the data acquisition system.

For the tire radial model shapes, the experimental data from the Tire Model Performance Test program (TMPT) is adopted. The TMPT program introduces a standard set of test procedures to evaluate the performance of tire models in conjunction with multibody system (MBS) vehicle models. These tests are divided into model capability tests and validation tests. The capability tests are designed to study the qualitative behavior of the tire, and show the physical plausibility of using the model. The validation tests contain the experimental test results for some steady-state and dynamic measurements [10]. It should be noted that similar definitions and arrangements for principal axis and force measurements are considered as the basis for constructing the current FEM model.

For the tire torsional modes, the modal analysis data performed on the modal test rig at the University of Pretoria was incorporated. The test setups for unconstrained and constrained tire configurations are shown in Figure 4. The Michelin LTX 235/85R16 tire was mounted horizontally on a hub with the UP VDG Wheel Force Transducer and KMT telemeter. A 100 kN hydraulic actuator with a 100 kN load cell was mounted horizontally. The tests were aimed at determining the frequency of the torsional modes of the test tire at different inflation pressures. The modes

were determined for a free rotation tire at an inflation pressure of 0 kPa, 100 kPa, and 200 kPa. Additional tests were conducted with the tire preloaded/constrained at 5, 20 mm and 30 mm tire deflection at the same inflation pressures as for the free rotating wheel, as shown in Figure 4 (a).

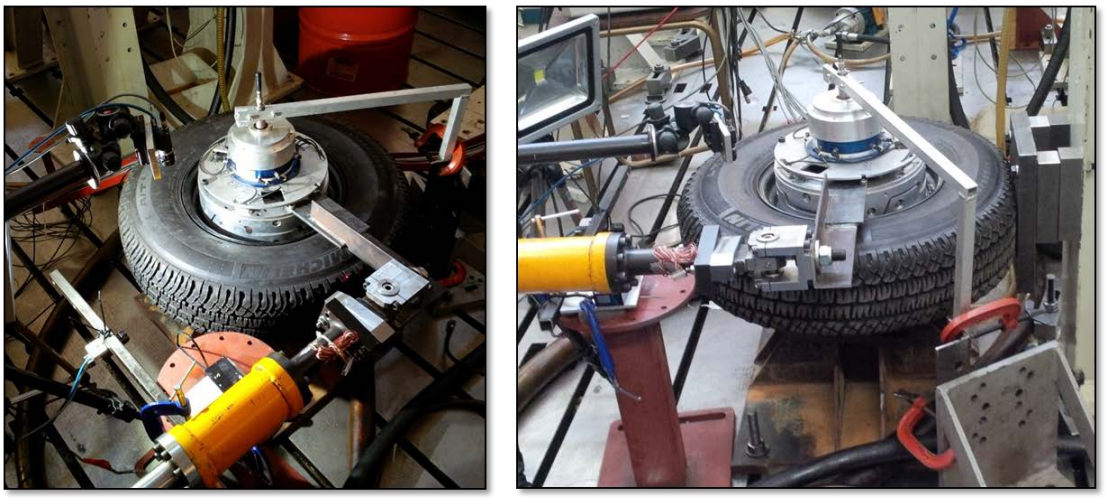

Figure 4: The modal analysis test rig at the University of Pretoria; (a) setup for unconstrained tire (b) setup for constrained tire

High-speed cameras were used to record the movement of the tire at 250 Hz. One camera was positioned perpendicular to the tread pattern. A second camera was positioned perpendicular to the sidewall. During the constrained tests, the sidewall movement was captured in the constrained and the unconstrained areas. A trigger channel was generated to synchronize the photographs with the sampling frequency of the data acquisitioning system.

Figure 5: Camera view for the (a) tire tread camera (b) tire sidewall camera

The actuator was controlled in displacement mode and supplied with a sinusoidal signal with 1 mm amplitude. The frequency of the sinusoidal input was swept from 0 Hz to 40 Hz and 45 Hz for the free rotating wheel and preloaded tests respectively. For each test setup 3 runs are conducted per test file. The first run was a slow sweep from 0 Hz to 40 Hz or 45 Hz. The second run was a fast sweep from 15 Hz to 40 Hz or 45 Hz. The third run was a slow sweep from 15 Hz to 40 Hz or 45 Hz. The frequency sweeps were conducted by hand on the actuator controller at an average sweep rate of 1.5 Hz/sec and 0.15 Hz/sec for the fast and slow sweeps, respectively. An Acuity AR700-RP laser (SN) was used to measure the rotational displacement of one of the tread blocks.

2. Quasi-static Loading Test

The cleat test experimental data used for studying the tire radial behavior was performed in cooperation with the Vehicle Dynamics Group at the University of Pretoria. The tests were aimed at characterizing the vertical stiffness of the Michelin LTX 235/85R16 tire on a flat plate and for various cleats at 100 kPa and 200 kPa tire gauge pressure at 0°, 3°, and 6° camber. The test tire was mounted on a pedestal with the UP VDG Wheel Force Transducer and KMT telemetry. A 16 kN hydraulic actuator with a 20 kN load cell was mounted horizontally. A single test at 0 kPa tire gauge pressure at zero camber was done with a flat plate to characterize the tire carcass stiffness with no air in the tire. A road profiling laser was mounted on the wheel load cell to measure the displacement of the plate or cleat pressing the tire. A camera was used on some of the tests to record the deformation of the tire. A trigger channel was generated to synchronize the photographs with the sampling frequency of the data acquisitioning system.

Two sets of tests were performed, at 100 kPa and 200 kPa tire gauge pressure and 0°, 3°, and 6° camber. The first set of tests was on a flat glass plate to determine the tire's vertical stiffness as a function of displacement. A camera was mounted beneath the glass plate to determine the contact patch shape and area. The image from the camera was used to construct the Bitmap image of the contact patch. A ruler was placed near the contact patch area for scaling the image to proper dimensions during the post-processing. The contact patch area was calculated from this image, as shown in Figure 6. The comparison between the estimated contact patch area values at 0°, 3°, and 6° camber angles and experimental results is discussed in Section 1.4.

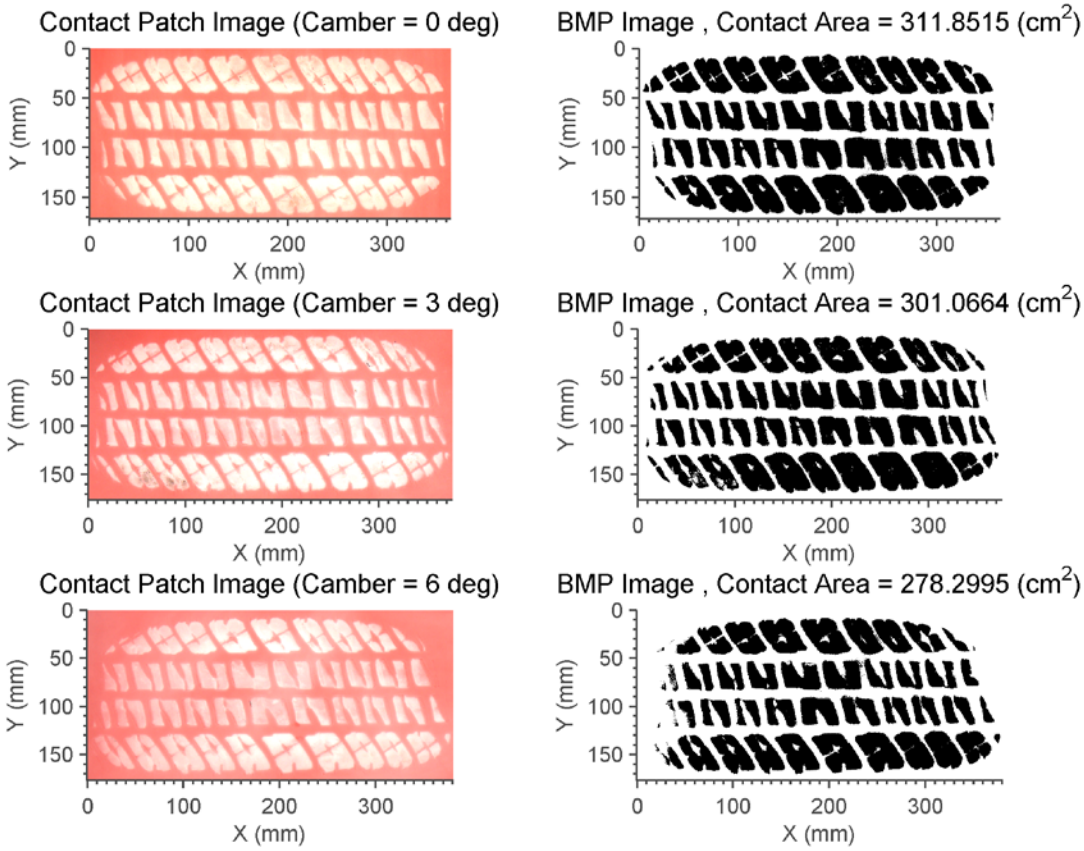

Figure 6: (Left) tire contact patch image at different camber angles (Right) corresponding Bitmap image with the calculated contact area

The second set of tests was conducted on 25 mm and 32 mm cleats mounted on a flat steel plate. The cleats were mounted transversely, longitudinally, and at a 45° angle, as shown in Figure 7. The quasi-static cleat test data was used for tire model parameter estimation in radial direction and model validation.

Figure 7: Quasi-static cleat test at different cleat orientations (a) longitudinal; (b) 45°; (c) transverse

4. Tire Modal Analysis

For the modal analysis test the tire was excited using a dynamic force; dynamic acceleration signals were measured at multiple locations around the tire circumference. This method is called the Single Input Multiple Output technique (SIMO). The Frequency Response Functions (FRFs) were obtained using the following function:

$$H_i = \frac{S_{FX_i(\omega)}}{S_{FF_i(\omega)}} \tag{2}$$

Where $S_{FX_i}(\omega)$ is the averaged crossed spectral density and $S_{FF}(\omega)$ is auto spectral density of the excitation force. The input excitation was applied to the tire using a hand-held excitation hammer. In this approach, it is challenging to control the intensity and direction of impacts precisely. The coherence function was exploited for each set of measurement signals to assess the validity of measurements:

$$\Gamma_i(\omega) = \sqrt{\frac{\left|S_{FX_i(\omega)}\right|^2}{S_{X_iX_i(\omega)}S_{FF(\omega)}}} \tag{3}$$

Where $S_{X_iX_i}(\omega)$ is auto spectral density at the i^{th} measurement location. Using the frequency response functions, the natural frequencies were identified from the location of the peaks and the damping values could be calculated from the width of the peaks. The natural frequencies and damping values for the radial modes (R) and transverse modes (T) of the unloaded, non-rotating tire were compared to the experimental values obtained from the TMPT data. The results are shown in Table 1.

Table 1: Comparison between modal analysis simulation test results and experimental data.

Modes	Natural Freq. (Hz)			Damping %		
	ABAQUS	Test	Error	ABAQUS	Test	Error
T0	47.54	47.20	0.72	0.023	0.021	9.52
T1	55.85	61.40	9.04	0.031	0.029	6.9
R0	79.35	81.77	2.96	0.066	0.068	2.94
R1	87.60	97.35	10.01	0.041	0.044	6.82
T2	104.68	116.02	9.77	0.038	0.036	5.56
R2	124.74	122.93	1.47	0.027	0.032	15.63
R3	145.17	149.47	2.87	0.02	0.024	16.67
R4	165.48	176.64	6.31	0.021	0.024	12.5

It can be seen that in most of the modes, the FEM model results correlate with the experimental data within a reasonable error margin. Meanwhile, the model slightly underestimates most of the natural frequencies and radial damping values; on the other hand, it overestimates the transverse damping values. The natural frequencies and damping values are further processed in order to find the force elements, stiffness and damping values in different directions (lateral, radial, longitudinal, inner element, etc.).

4.1 Estimating Tire Mode Shapes

The tire mode shapes are related to the gain of the resonance frequencies. The gains can be specified from the height of the peaks of the frequency response functions. In order to estimate the tire mode shapes, the frequency response function should be decomposed into individual response function corresponding to each resonance natural frequency. The structure dynamic response at each resonance peak is modeled using a single degree of freedom system SDOF. This simplifying assumption is applicable because the resonance frequencies are well separated. The FRF of a SDOF has the following form:

$$S_n(\omega) = \frac{\omega_{0n}^2}{\omega_{0n}^2 + 2jc_n\omega\omega_{0n}^2 - \omega^2} \quad (4)$$

Where ω_{0n} is natural frequency of the SDOF system and c_n is the corresponding damping. The total estimated response function of the tire at point i^{th} is equal to the sum of all modal response functions multiplied by modal amplitudes $a_{i,n}$:

$$H_i^{est}(\omega) = \sum_{n=1}^{m} a_{i,n} S_n(\omega) \tag{5}$$

Where n and m represent the mode number and number of modes used respectively. The modal amplitude is calculated using the i^{th} experimental modal response $H_i^{\exp}(\omega)$:

$$a_{i,n} = \frac{\overline{S_n}(\omega)^T H_i^{exp}(\omega)}{\overline{S_n}(\omega)^T S_n(\omega)} \qquad (0.95\omega_{0n} < \omega < 1.05\omega_{0n}) \tag{6}$$

To evaluate the fitted frequency response function $H_i^{est}(\omega)$, we define the error function $E_{i,n}$ as:

$$E_{i,n} = \left\| H_i(\omega) - a_{i,n} S_n(\omega) \right\| \quad (0.95\omega_{0n} < \omega < 1.05\omega_{0n}) \tag{7}$$

And the total error is found as:

$$E_n = \sum_{j=1}^{n_{imr}} E_{n,i} \tag{8}$$

Where n_{imr} is the total number of measured frequency response functions. Table 2 and Table 3 present the tire mode shapes in radial and transverse directions corresponding to the natural frequency listed in Table 1 [3].

Table 2: Tire radial modes

Modes	Front View	Top View
R0	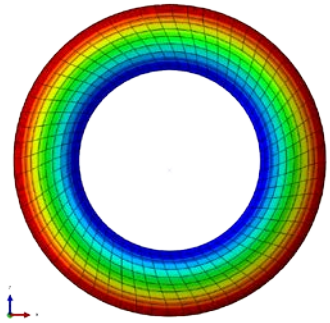	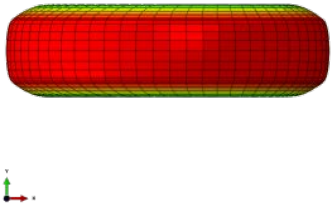
R1	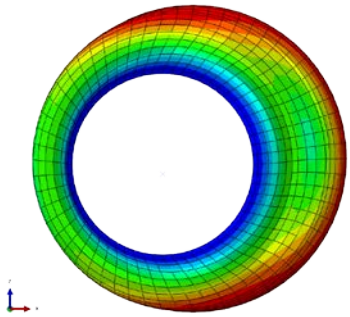	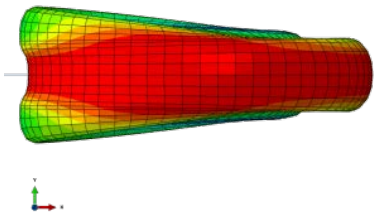
R2	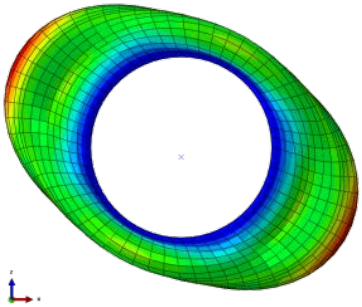	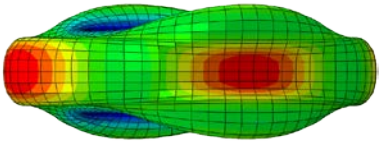
R3	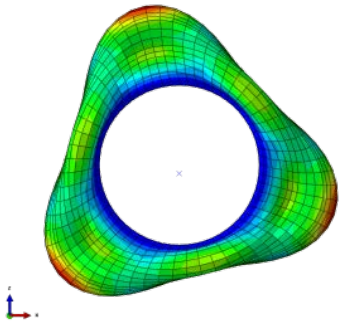	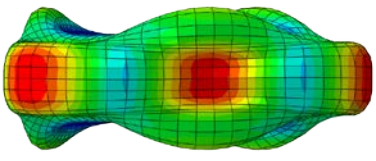

Table 3: Tire transverse modes

M	Front View	Top View
T0	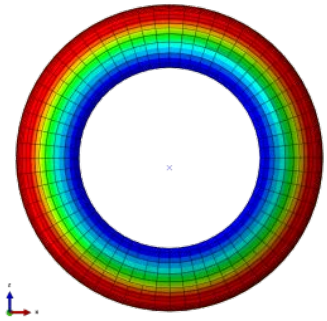	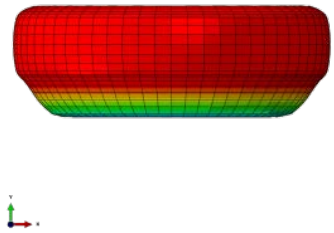
T1	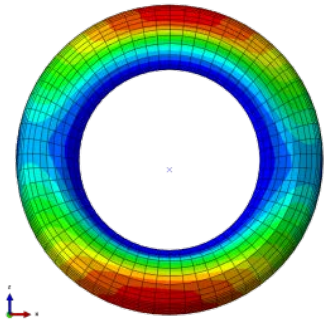	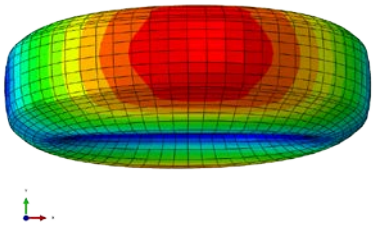
T2	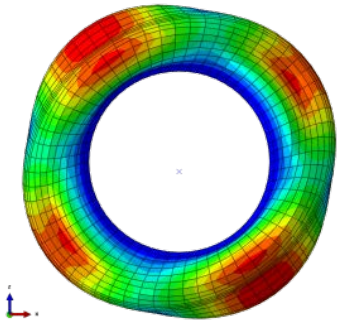	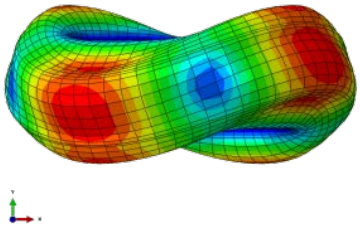
T3	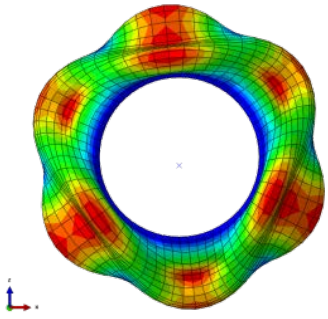	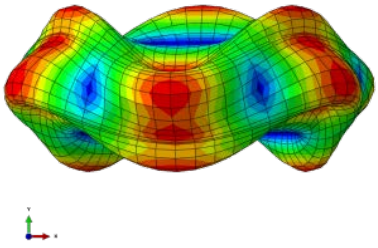

5. Theoretical Tire In-plane Vibrational Analysis

In order to calculate the theoretical tire in-plane natural frequencies and damping values, the tire can be simplified as an elastic ring on an elastic foundation. In this case, the equations of motion can be written as:

$$-\frac{EI}{a^4}\left(\frac{\partial^2 u_\theta}{\partial\theta^2}-\frac{\partial^3 u_r}{\partial\theta^3}\right)-\frac{EI}{a^2}\left(\frac{\partial^2 u_\theta}{\partial\theta^2}-\frac{\partial^3 u_r}{\partial\theta}\right)+k'_\theta u_\theta+m\ddot{u}_\theta=0 \tag{9}$$

$$-\frac{EI}{a^4}\left(\frac{\partial^3 u_\theta}{\partial\theta^3}-\frac{\partial^4 u_r}{\partial\theta^4}\right)+\frac{EI}{a^2}\left(\frac{\partial u_\theta}{\partial\theta}+u_r\right)+k'_r u_r+m\ddot{u}_r=0 \tag{10}$$

Where:

$$k'_\theta=k_\theta b \tag{11}$$

$$k'_r=k_r b \tag{12}$$

$$m=\rho A+\frac{1}{3}\rho_F h_F b \tag{13}$$

The parameters k_θ and k_r are the foundation stiffness values in radial and tangential directions, b is the width of the ring, h is the thickness of the ring, $A=bh$ is the cross area, and $I=bh^3/12$ is the area moment of inertia. The radial and tangential solutions for the equations of motion are denoted as:

$$u_r(\theta,t)=A_n\cos n(\theta-\phi)e^{j\omega t} \tag{14}$$

$$u_\theta(\theta,t)=B_n\cos n(\theta-\phi)e^{j\omega t} \tag{15}$$

Substituting above solutions in the equations of motion (EOM) will result in:

$$\begin{bmatrix}\alpha_{11}-m\omega_n^2 & \alpha_{12}\\ \alpha_{21} & \alpha_{22}-m\omega_n^2\end{bmatrix}\begin{Bmatrix}A_n\\ B_n\end{Bmatrix}=0 \tag{16}$$

Where:

$$\alpha_{11}=\frac{n^4EI}{a^4}+\frac{EI}{a^2}+k'_3 \tag{17}$$

$$\alpha_{12}=\alpha_{21}=\frac{n^3EI}{a^4}+\frac{nEI}{a^2} \tag{18}$$

$$\alpha_{22}=\frac{n^2EI}{a^4}+\frac{n^2EI}{a^2}+k'_\theta \tag{19}$$

Setting the determinant to zero to have a nontrivial solution provides:

$$\omega_n^4 - K_1\omega_n^2 + K_2 = 0 \tag{20}$$

Where:

$$K_1 = \frac{n^2+1}{a^2 m}\left(\frac{n^2 EI}{a^2} + EA\right) + \frac{k_r' + k_\theta'}{m} \tag{21}$$

$$K_2 = \frac{n^2(n^2-1)^2}{a^6 m^2} E^2 IA + \frac{k_r' k_\theta' + k_r'\left(\frac{n^2 E}{a^2}\right)\left(\frac{I}{a^2}+A\right) + k_\theta'\left(\frac{E}{a^2}\right)\left(\frac{n^4 I}{a^2}+A\right)}{m^2} \tag{22}$$

The natural frequencies for the n^{th} mode are:

$$\omega_{n1}^2 = \frac{K_1}{2}\left(1 - \sqrt{1 - 4\frac{K_2}{K_1^2}}\right) \tag{23}$$

$$\omega_{n2}^2 = \frac{K_1}{2}\left(1 + \sqrt{1 - 4\frac{K_2}{K_1^2}}\right) \tag{24}$$

The natural frequency set ω_{n1} is associated with the ring modes where the radial motion dominates. On the other hand, the higher natural frequency set ω_{n2} corresponds to ring modes where the tangential displacement is more significant. Therefore, by measuring the frequencies ω_{n1} and ω_{n2} for the first radial and torsional modes of the tire we can calculate k_θ and k_r.

6. Parameter Estimation Procedure

The parameter estimation process is started by finding initial values for the tire structure model parameters. These initial values are used in a non-linear curve-fitting process as initial guesses for finding a set of model parameters that can result in the highest correlation between the model estimations and the test data. The measured tire modal frequencies have been utilized to estimate tire parameters corresponding to in-plane tire dynamics. The calculated tire model parameters are included in Table 4.

Table 4: Tire model parameters

Parameter	Symbol	Value	Unit
Tire bending stiffness	*EI*	3.654	N/m^2
Tire extensional stiffness	*EA*	4.12 E6	N/m^2
Sidewall tangential stiffness	K_{st}	3.234 E5	N/ m^2
Sidewall radial stiffness	K_{sr}	8.168 E4	N/ m^2
Sidewall lateral stiffness	K_{sl}	2.212 E5	N/ m^2
Belt tangential stiffness	K_{bt}	3.544 E6	N/ m^2
Belt radial stiffness	K_{br}	5.481 E4	N/ m^2
Belt lateral stiffness	K_{bl}	6.990 E6	N/ m^2

Tire Model Parameter Estimation in Radial Direction

In order to find the sidewall and the belt radial stiffness values, the cost function for the optimization problem was defined as:

$$\min_{K_{sr},K_{br}} \sum_i \left(\Omega\left(K_{sr}, K_{br}, Z_{ground}, Camber\right) - F_z\right)^2 \tag{25}$$

Where K_{sr} is the sidewall radial stiffness, K_{br} is the belt radial stiffness, and F_z is the vertical load at the wheel center. The vertical loading simulations were conducted by applying the camber angle, fixing the tire at the spindle, placing the cleat at the test configuration angle and adjacent to the tire circumference, and vertically displacing the "ground". Next, a smoothing function was fitted to the vertical force versus displacement experimental data at different test configurations. (The cleat test experiment was performed in collaboration with the University of Pretoria, S. Africa). This process results in nine different force-displacement curves for 3 camber angles and 3 cleat configurations. The fitted line to the experimental data is shown as a blue line in Figure 8, Figure 9, and Figure 10. These nine data sets are concatenated and used in the described optimization routine to find tire model sidewall and belt radial stiffness values.

The parameterized tire structure model was used to estimate the vertical force at the wheel center with model inputs from the experimental setup including the tire camber angle, cleat orientation, and vertical displacement. The estimated vertical load signals at different test conditions are shown in Figure 8, Figure 9, and Figure 10.

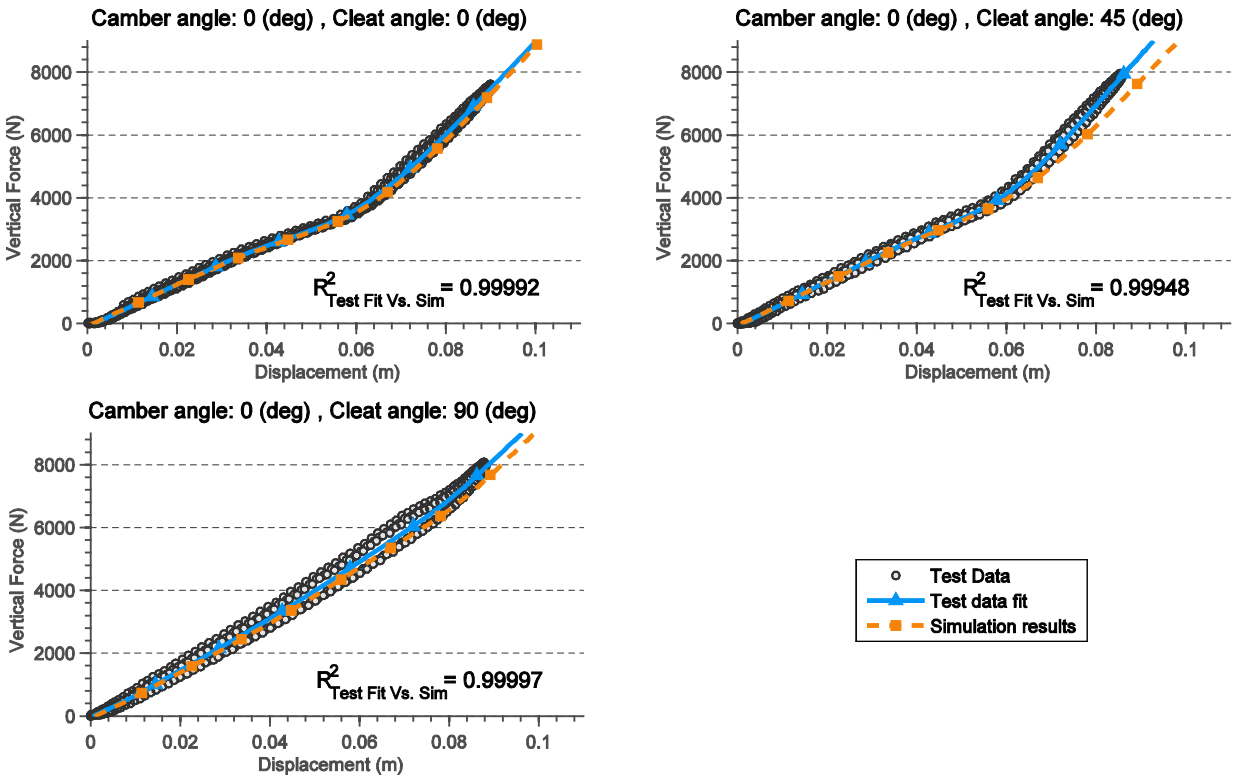

Figure 8: Tire quasi-static loading test with rectangular cleat setup at 0°, 45 °, and 90° orientations and at 0° camber angle

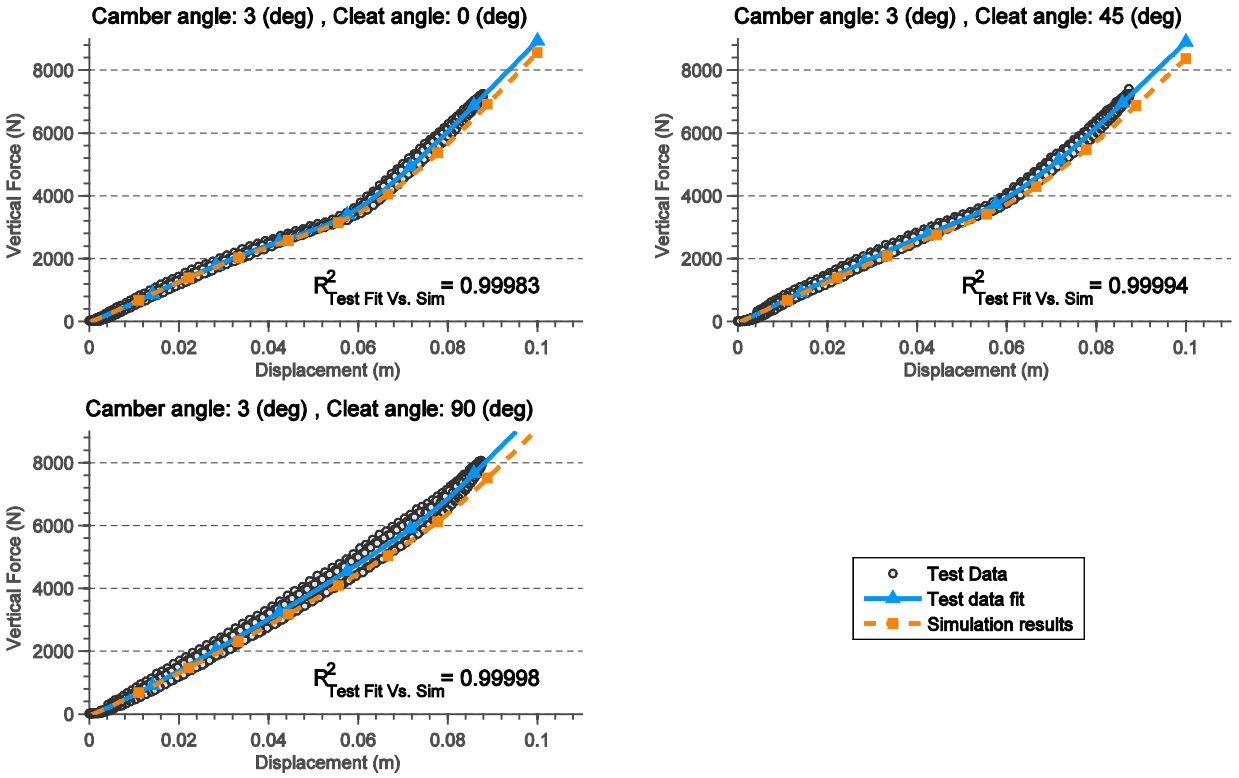

Figure 9: Tire quasi-static loading test with rectangular cleat setup at 0°, 45 °, and 90° orientations and at 3° camber angle

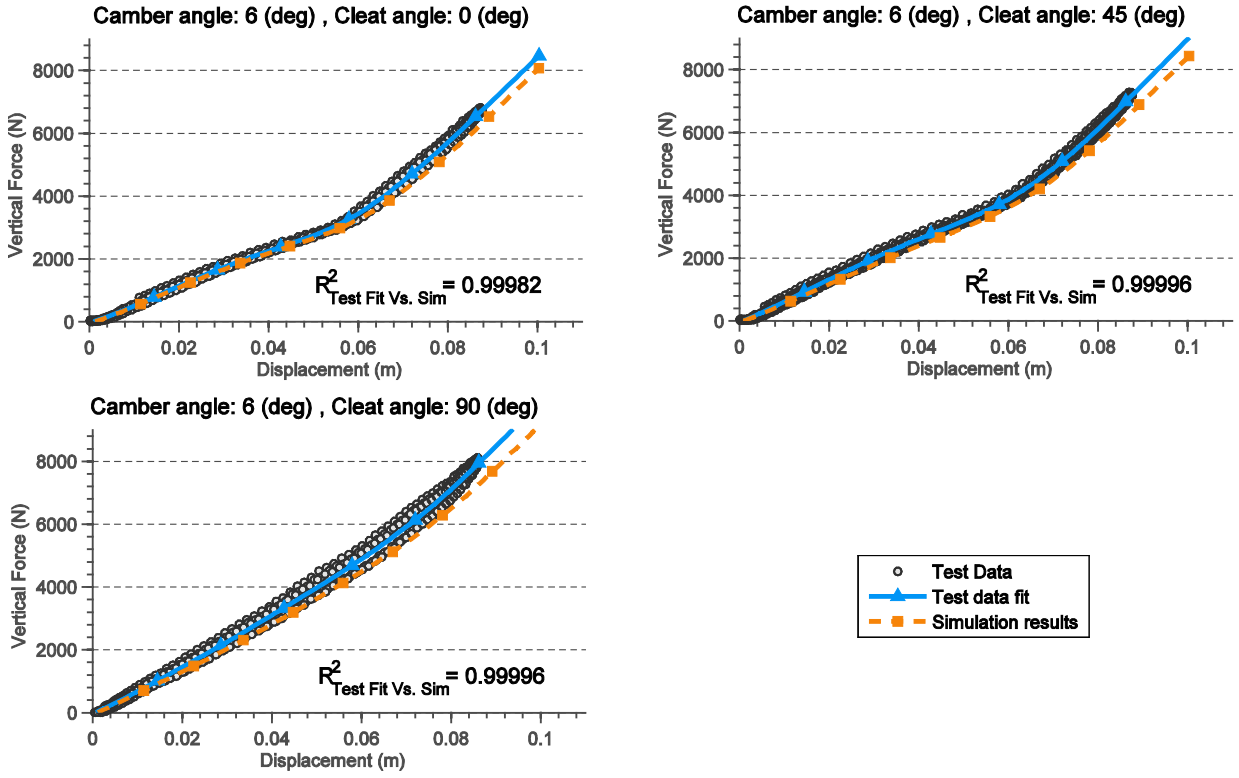

Figure 10: Tire quasi-static loading test with rectangular cleat setup at 0°, 45 °, and 90° orientations and at 6° camber angle

In order to measure the accuracy of force-displacement estimations, the simulation results were correlated with experimental results at identical input conditions, and the correlation coefficient R^2 is shown on the figures. It can be seen that using the final optimized tire sidewall and belt radial stiffness values, the estimated normal loads at the wheel center during the cleat test loading at different test conditions have high correlation (R^2 near unity) with experimental data.

Tire Model Contact Area Validation

During the tire vertical loading experiments, a series of test runs were conducted on a flat glass plate to determine the tire's contact patch area. A camera was mounted beneath the glass plate to capture the contact patch shape and area. As it was discussed earlier, the contact patch images were converted to bitmap images, which were ultimately used to calculate the tire contact patch area. The calculated contact patch area values at the end of the loading process on a flat plate at three values of tire camber angles are shown in Figure 6. Tire model simulations were conducted with the input configurations similar to the test setup in order to evaluate the contact patch area. The estimated area calculations for the three values of tire camber angle are included in Figure 11.

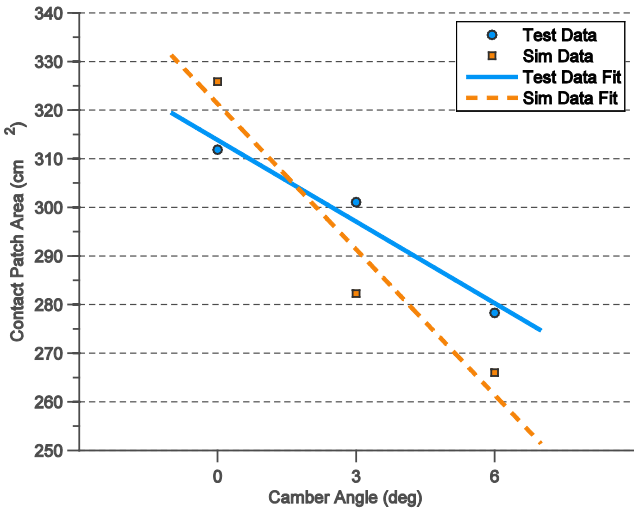

Figure 11: Contact patch area comparison between model estimation and experimental results

The developed tire model overestimates the contact patch area at zero camber angle. This was expected because the tread pattern is not included in the simulation model. In other words, the sipes and grooves in the tread pattern reduce the effective contact patch area during the experiments. Moreover, at non-zero camber angles, the tread pattern features enable the belt package to deform extensively under loading, which results in uniform contact over

the surface, whereas for the simulated tire model, the belt package behaves as a membrane that pivots over the contacting sidewall, and, consequently, has less uniform contact with the ground surface. This makes the estimated tire contact patch area less than the calculated value from the experiments at non-zero camber angles.

Tire Model Parameter Estimation in Longitudinal and Lateral Directions

As it was discussed in Part II [2], the total deformation of the brushes used in the rigid terrain contact model, relative to the ground surface, depends on the brush stiffness as well as the tire sidewall and belt stiffness values in longitudinal and lateral directions. Therefore, a set of model parameters for the integrated tire-terrain models should be identified that results in accurate contact shear force estimations. The terrain model, which was parameterized previously, was integrated with the HSSTM to conduct cornering and braking/accelerating simulations. During the braking/accelerating tests, the tire slip ratio was changed from -30% to 30% to -30% at different levels of normal load. The tire steady-state force generation characteristics as well its transient dynamic behavior are involved in this type of simulation. The following cost function was defined to find the model parameters in longitudinal direction:

$$\min_{K_{st},K_{bt},C_{st},C_{bt}} \sum_i (\Omega(K_{st}, K_{bt}, C_{st}, C_{bt}, \kappa) - F_z)^2 \tag{26}$$

Where K_{st} is the sidewall tangential stiffness, K_{bt} is the belt tangential stiffness, C_{st} is the sidewall tangential damping, C_{bt} is the belt tangential damping, κ is slip ratio, F_z is the vertical load at the wheel center, and F_x is the longitudinal force at the wheel center. The optimization algorithm was applied to the experimental data to find a set of tangential model parameters that can minimize the model longitudinal force estimation error. With this set of model parameters, simulations were conducted at the test condition to estimate the longitudinal forces at different normal load levels. The experimental and the calculated tire longitudinal forces are shown in Figure 12.

For the cornering case study, the tire slip angle was swept from -12° to 12° to -12° at different levels of normal load. For the lateral parameter estimation case study, the following cost functions was introduced:

$$\min_{K_{sl},K_{bl},C_{sl},C_{bl}} \sum_i \left(\Omega(K_{sl}, K_{bl}, C_{sl}, C_{bl}, \alpha) - F_y\right)^2 \tag{27}$$

Where K_{sl} is the sidewall lateral stiffness, K_{bl} is the belt lateral stiffness, C_{sl} is the sidewall lateral damping, C_{bl} is the belt lateral damping, α is slip angle, F_z is the vertical load at the wheel center, and F_y is the lateral force at the wheel center. Similar to the tangential case study, the optimization algorithm was incorporated to find the lateral

model parameters that minimize the error of lateral force. With this parameter set, the lateral tests were simulated at the similar normal load and slip angle inputs. The lateral force curves from experimental data as well as model estimations are shown in Figure 12.

The aligning moment and the overturning moment curves are plotted in Figure 13. It can be seen that terrain model force and moment estimations are in good agreement with the experimental results. The hysteresis loop in the forces and moments curves is associated with the tire transient effect. This phenomenon causes the forces and moments curves to not follow the same trend during the increasing and the decreasing slip value changes, as can be seen in Figure 12 and Figure 13.

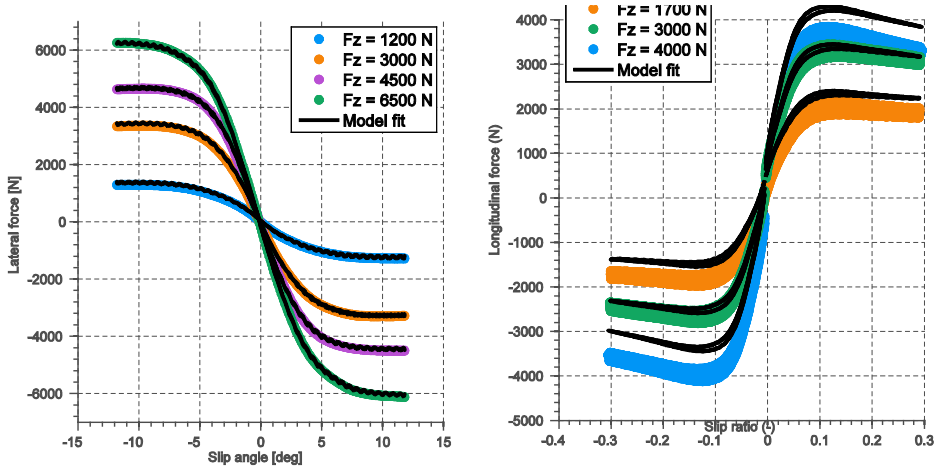

Figure 12: Lateral and longitudinal forces during tire interaction with rigid terrain

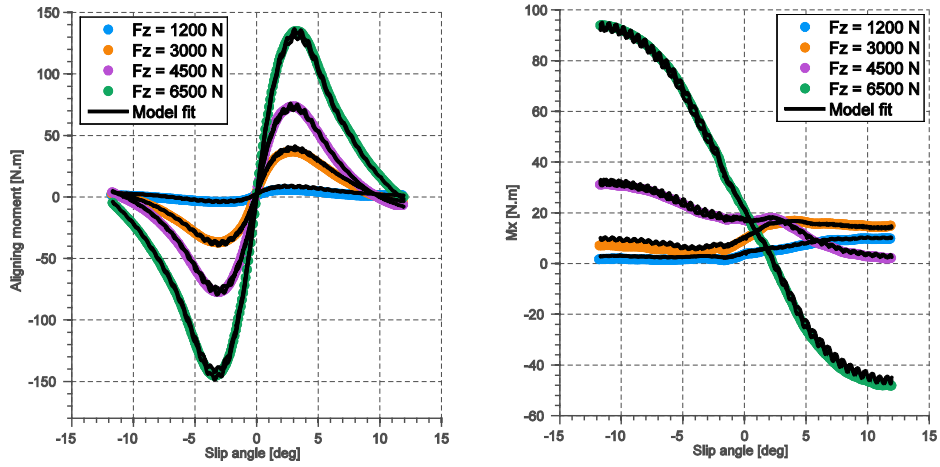

Figure 13: Aligning and overturning moments during tire interaction with rigid terrain

The final calculated tire model parameters are included in Table 5.

Table 5: Tire model final optimized parameters

Parameter	Symbol	Value	Unit
Sidewall tangential stiffness	K_{st}	2.921 E5	N/ m^2
Sidewall radial stiffness	K_{sr}	8.965 E4	N/ m^2
Sidewall lateral stiffness	K_{sl}	3.251 E5	N/ m^2
Belt tangential stiffness	K_{bt}	3.129 E6	N/ m^2
Belt radial stiffness	K_{br}	5.520 E4	N/ m^2
Belt lateral stiffness	K_{bl}	7.103 E6	N/ m^2

Validation studies

In the following sections, the tire structure model dynamic characteristics are validated with the dynamic cleat test data. Next, the tire and the soft soil terrain models are integrated in the HSSTM simulation package and are used to simulate the Terramechanics test rig conditions.

Dynamic cleat test simulations

The dynamic behavior of the tire structure model should be studied for rigid terrains with obstacles. In this regard, a cleat test simulation was conducted using the HSSTM, and the results were compared with three commercially-available tire models, including MF-Swift, CarSim internal tire model, and Delft tire model. For the cleat test maneuver, a 225/60 R18 tire was constrained laterally, and it was towed at a speed of 40 km/h over a sharp rectangular cleat, which is 7 m wide, 0.40 m long, and 0.035 m high. The tire transient behavior in the frequency range of under 10 Hz was dominant in this test, and, consequently, the linear tire structure model was used for the simulations.

The MF-Swift tire model represents the tire structure with a rigid ring that is suspended on an elastic foundation. This rigid ring has a single-point contact with terrain. The effect of the tread modulus is modeled as residual spring and dampers that are connected to the contact point. The normal load, slip, camber angles, and slip ratio at the tire/terrain contact point are the main inputs to the ground interaction model, which outputs the forces and moments at the center of the contact patch. The Delft tire model is an implementation of the Magic Formula tire

model, which models the tire structure with a single spring having a point contact with terrain. The CarSim internal tire model uses the same methodology as the Delft tire model for characterizing the tire structure stiffness, and calculating the normal load the location of tire contact with ground. The CarSim internal tire model uses table interpolation/extrapolation for calculating tire forces and moments at the center of the contact patch.

In order to estimate the HSSTM structure model parameters, the tire natural frequencies and damping values from the literature [11] were used as inputs to the parameters estimation procedure developed for the in-plane elastic tire model. The tire parameters for other benchmarked tire models were selected from the CarSim available database for the same tire. The wheel center height and the longitudinal and vertical forces at the wheel center are plotted in Figure 14 against the wheel longitudinal displacement.

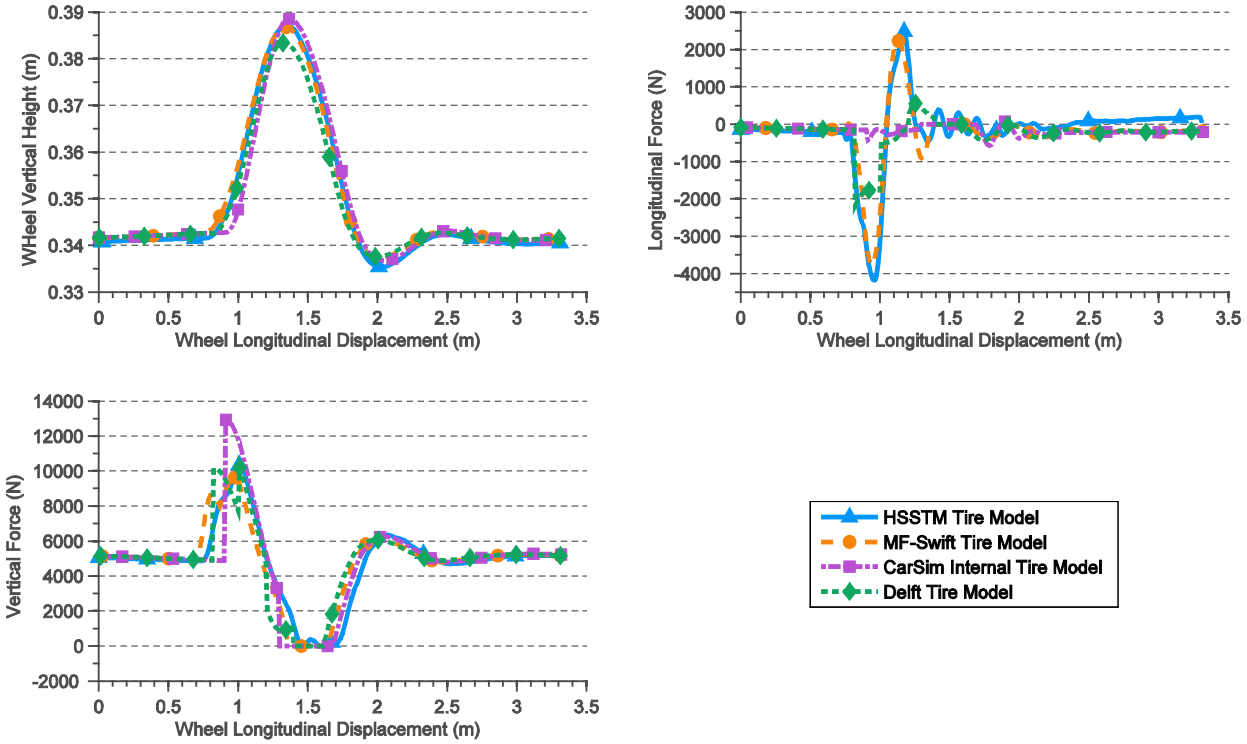

Figure 14: Cleat test simulation results for four tire models: HSSTM tire model, MF-Swift Tire Model, CarSim Tire Model, Delft Tire Model

In Figure 14, the vertical force signals at the wheel center estimated by CarSim internal tire model and Delft tire model suddenly increases when tire encounters the cleat. This impulsive behavior is due to the simplistic single spring model used in these models, which do not provide any in-plane damping or accurate enveloping characteristics. Failure to evaluate the normal force (one of the main inputs to the force and moments estimation module) correctly results in inaccurate longitudinal force calculation. On the other hand, the MF-Swift model, which

was validated for this tire choice and test configuration in [11], has a good performance in estimating the tire vertical position and longitudinal and vertical forces. The developed HSSTM has a very high correlation with the performance of the MF-Swift model. This emphasizes the capability of the HSSTM in characterizing the dynamic tire behavior, such as enveloping over a cleat.

Terramechanics test rig experiments

In order to compare model longitudinal force estimations with experimental results, straight line tests were conducted in Terramechanics test rig [12-14] at Virginia Tech. During these tests, the tire slip angle, camber angle, normal load, and tire pressure were kept constant while the tire slip ratio was varied. The main tire model input signals including slip angle, slip ratio, camber angle, and normal load were measured and provided to the developed simulation environment to estimate the F&M at wheel center. The overview of the described validation test bench is presented in Figure 15.

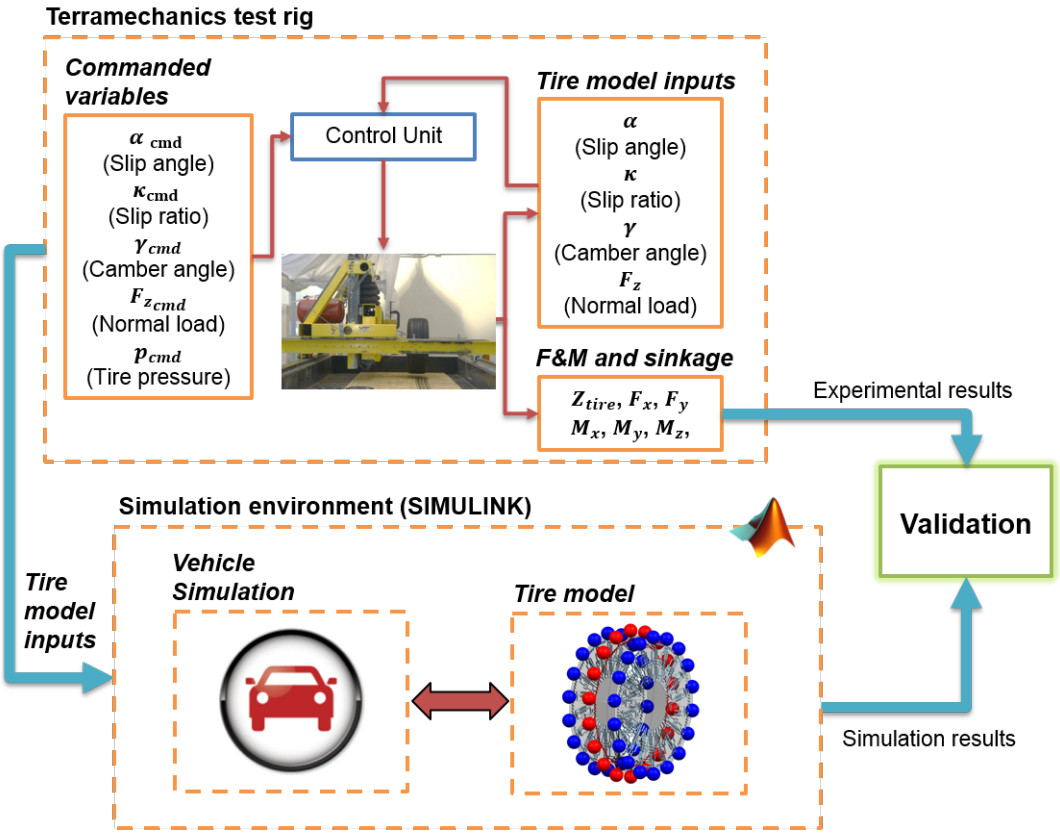

Figure 15: Validating the tire model results using experimental data from Terramechanics test rig

The forces and moments at the wheel spindle directly affect the vehicle handling and rollover behavior. The longitudinal and lateral forces are the quantities of interest, because they influence the planar motion of the vehicle. All forces and moments were measured at the spindle, and the wheel sinkage was calculated using a novel method developed by Naranjo [12,13]. In this method, the wheel sinkage was calculated by post-processing the data from the sensors that are implemented inside the tire cavity. These sensors were integrated units composed of a position sensitive detector (PSD), five infrared emitting diodes (IREDs), and a signal processing circuit. The similar test configuration was designed using the developed tire model platform, and simulation runs were conducted at the input conditions identical to the experimental test setup. The tire used for conducting the tests was the Michelin LTX 235/85R16. The tire tread was buffed in order to study the performance of the treadles tire, as it was considered to be closer to the HSSTM implementation, which did not account for the tire tread pattern.

For the longitudinal case study, the slip angle and the camber angle were set to zero, the normal load was maintained near 4000 N, and the slip ratio was controlled at nine different levels using the applied torque to the wheel at longitudinal speed of 0.5 m/s. The test data was collected and reported by Naranjo [12,13] on an upland sandy loam with the tire inflated at its nominal pressure. The mechanical properties of this terrain are presented in Table 6.

Table 6: Mechanical properties of the mineral terrain used in the rig [15].

Soil Type	Bekker's equation			Moisture content (%)	Shear characteristics			
	$n\,(-)$	k_c $\left(\frac{kN}{m^{n+1}}\right)$	k_φ $\left(\frac{kN}{m^{n+2}}\right)$		RS $\left(\frac{cm}{s}\right)$	c (kPa)	φ $(\deg)$	K (cm)
Upland sandy loam	0.65	22.7	1325	25.2	2.4	1.95	22.3	4.28

Three test runs were conducted at each pre-defined slip ratio level. The longitudinal force data sets (recorded at the spindle) at each slip ratio are averaged between the test runs, and plotted in Figure 16 (a) with their error bars. The horizontal error bars correspond to standard deviations in slip ratio measurements, and vertical error bars are associated with the standard deviations in force readings. It can be observed that at each commanded slip ratio value, the longitudinal force have some small variations, possibly due to changes in the measured slip ratio value and normal load, in addition to irregularities in the soil compaction.

Using the tire models input signals acquired from the test rig, the runs are simulated, and the results are plotted in Figure 16 (a). The developed model (HSSTM) can estimate the overall trend of the longitudinal force vs. slip ratio curve including the slope of the linear region and the location of the peak. The longitudinal force was calculated at the center of the wheel. The Nepean Wheeled Vehicle Performance Model, NWVPM [15], was used to simulate the explained test condition. This model considers the tire as a rigid structure and characterizes the terrain behavior with semi-empirical equations similar to ones that are used in HSSTM package. Therefore, NWVPM results are solely based on the empirical equations for wheel thrust, rolling resistance and sinkage. Comparing the output of two models shows that at low slip angles both models have good agreement with experimental data. When slip increases, the rigid wheel model estimated longitudinal force starts to deviate from the experimental data. This is due to the fact that the rigid wheel model does not account for the flat portion of the contact patch in which tire has the maximum relative velocity with the terrain, and consequently largest longitudinal force.

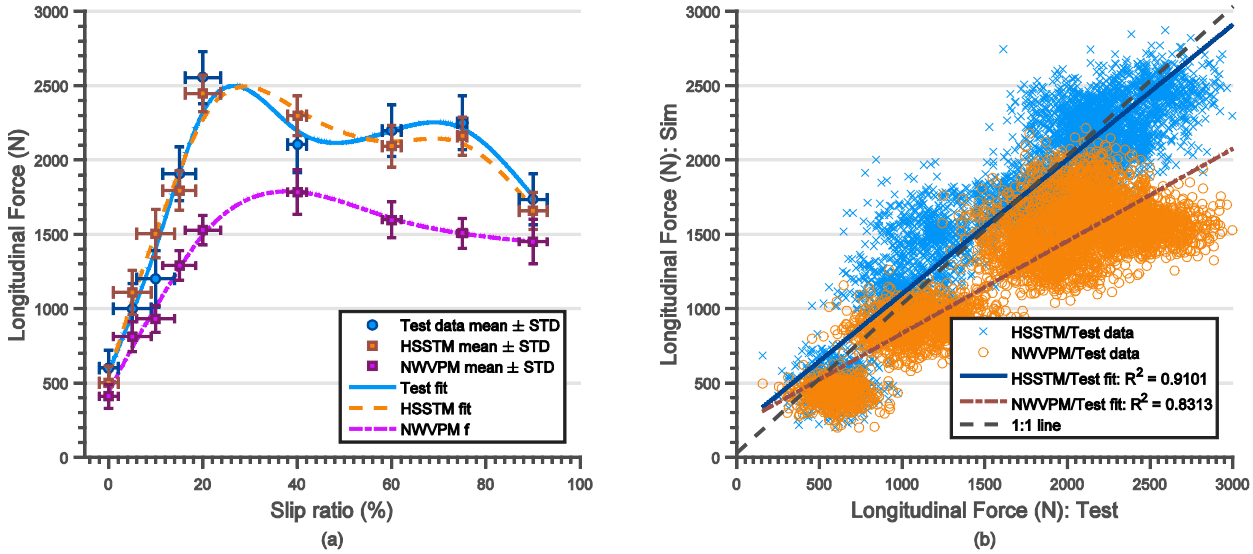

Figure 16: Longitudinal force at wheel center at different slip ratio levels (a) force vs. slip results including error bars (b) cross plot validation

Validation of the tire model response quantities versus the measurement data was done using cross plot validation charts. For every parameter, simulation results were plotted versus the test data across the entire simulation time span. The Y-value of every blue cross on the cross plot validation chart is the simulation result at the input condition identical to test condition and the X-value is the experimental output. The simulation and experimental output signals from all of the test runs were concatenated to form the entire data set. Next, a line was

curve-fitted to the resulted data points, and was plotted on the same figure. It should be noted that for better visualization only a reduced number of data points were shown in the cross plot validation plots.

The cross-plot validation results are shown in Figure 16 (b). To assess the quality of the match, curve-fitted line properties, including the slope, the intersection with the Y axis, and the coefficient of determination (R^2) are shown on the figures. For a perfect model, the slope and coefficient of determination R^2 for this linear line should be equal to one. The R^2 index is an indication of how the data is distributed around the curve-fitted line; so, for a completely scattered data, this value will become zero. As shown in Figure 16 (b), the developed model can perform adequately in estimating the longitudinal force across the entire range of slip ratio values.

The estimated sinkage values are compared with experimental results and NWVPM model results in Figure 17.

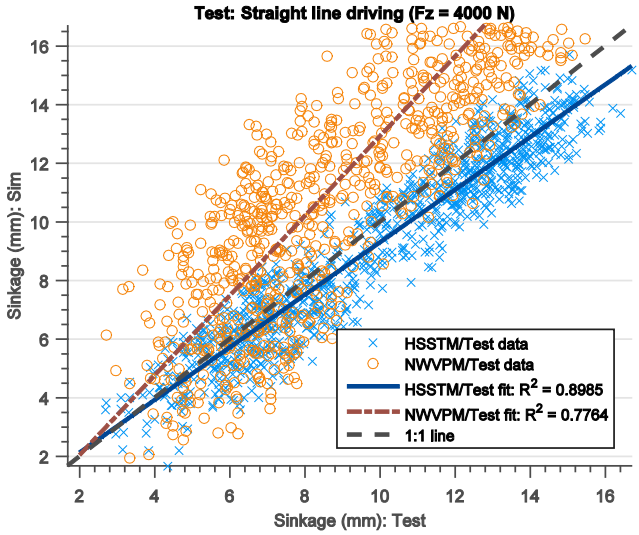

Figure 17: System response quantities cross-plot validation: wheel sinkage

The sinkage validation plot suggests that the HSSTM performs very well in estimating this parameter. The sinkage values range from low sinkage at zero slip ratio up to greater sinkage values at higher slips. The curve-fitted line in the sinkage plot starts to deviate from the 1:1 line as the sinkage increases, and always remains below the red dashed line. This means that at higher sinkage values, the measured sinkage value is greater than the simulation results. The higher sinkage values occur at higher slip values, at which time the tire starts to displace large volumes of soil particles and dig into the terrain. Considering the fact that the soil volume displacement model is not used in this simulation can justify the trend of the sinkage cross-plot results. The longitudinal force model has adequate performance in estimating the measurement data.

For comparison, the NWVPM had a good accuracy in estimating sinkage at low penetration depths corresponding to lower slip values. At higher sinkage values, the model fit deviated from the 1:1 line, and had lower R^2 values than the HSSTM, which indicates a lower model accuracy at these situations. This can be due to the fact that at higher loads the model considers a rigid wheel approximation for the tire structure. Therefore, the wheel must have a higher penetration into the terrain to have a higher contact patch length. On the other hand, in HSSTM at higher loading conditions (higher slip values), the tire structure deforms to achieve the larger contact patch (and consequently higher longitudinal forces), and this results in a smaller sinkage value.

Although test runs were performed in a straight line, the lateral force and the aligning moment values change during these maneuvers. This can be explained by considering the following facts: (1) when the tire is traveling on a rigid ground it produces a lateral force and an aligning moment. This results from the plysteer and the conicity in the tire construction. The effect of these manufacturing defects is modeled as a pseudo slip angle (for plysteer) and a pseudo inclination angle (for conicity). The pseudo slip angle and the inclination angle (camber angle) cause the residual lateral force and aligning moment to appear in straight line maneuvers; (2) The ground surface is not perfectly flat and does not have identical mechanical properties in all directions (non-isotropic).

To better study the tire model lateral behavior, cornering tests are conducted at free rolling condition (zero slip ratio), zero camber, and 5 levels of slip angle, while the normal load is maintained near 5000 N. The test data was collected by Jimenez [16] on the Terramechanics test rig. The lateral force measurements between the three test runs are averaged and plotted in Figure 18 (a) with their associated error bars.

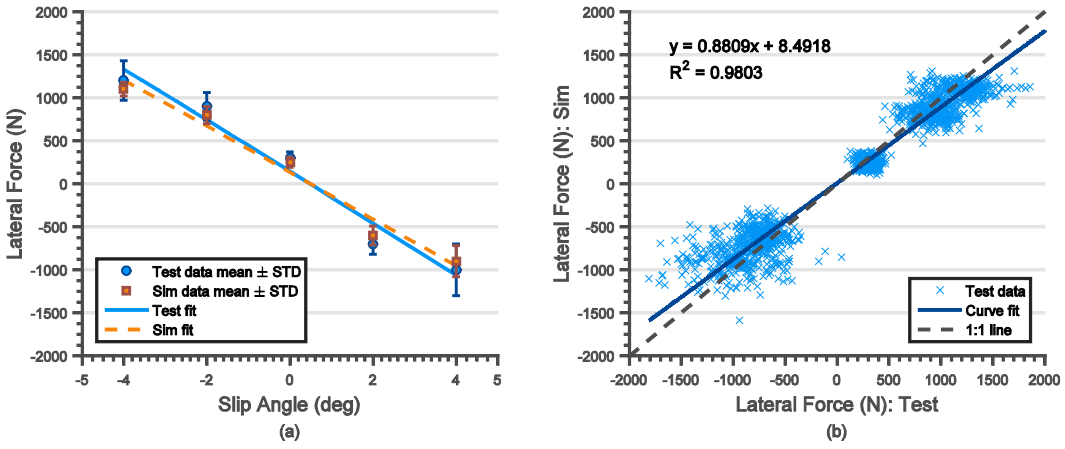

Figure 18: Lateral force at wheel center at different slip angle levels (a) force vs. slip results including error bars (b) cross plot validation

It can be seen that, at high slip angle values, the average values for the simulation data slightly deviate from the test data but their error bars have a substantial overlap. This is mostly due to the soil displacement at higher slip values. Additionally, the wheel carriage in the Terramechanics test rig is located relatively near the right wall of the experimental test rig. This causes the soil to pile up near the wall edges and produce a pressure gradient on the tire sidewall that shifts the generated lateral force values [17].

When the tire sinks into the ground, soil pressure distribution is applied to the tire sidewalls from the accumulated soil pile that is displaced out of the tire path. This force is known as bulldozing force, and contributes to the lateral force and, consequently, to the aligning moment generation.

Unlike the tire interaction with the rigid surface, which causes large lateral deformation in the tire structure, the tire-soil contact mostly results in the terrain deformation and soil displacement. The cross-plot correlation results for the lateral case study are plotted in Figure 18 (b) and indicate a high correlation between the model and experimental lateral forces. It should be mentioned that the lateral force estimation results were not compared with NWVPM, because this model cannot characterize tire dynamics in the lateral direction.

7. Conclusion

The HSSTM model parameterization study was conducted to find a set of model parameters that can minimize the error between the model simulation results and the experimental results. The individual test studies were done to obtain the tire model parameters in radial, tangential, and lateral directions.

Initially, from the modal analysis data, the input acceleration signal (from the input hammer), and output acceleration signals (from the accelerometers installed on the circumference of the tire) were used to construct the frequency response functions between the input-output points. Moreover, the tire mode shapes, natural frequencies, and damping values were extracted from the corresponding FRFs. In order to correlate the modal analysis results to tire in-plane dynamics, the tire structure was idealized as an elastic ring on an elastic foundation. The natural frequency and damping values for the theoretical model were calculated and related to the experimental data. As a result, the initial stiffness and damping values for the in-plane force elements used in the HSSTM were identified.

A least-square curve-fitting algorithm was used to find the model parameters in radial, longitudinal and lateral directions. The initially calculated model parameters were essential in having the optimization algorithm to converge to the final set of model parameters quickly. Quasi-static cleat loading tests were used to find the tire model sidewall

and belt radial parameters. The accuracy of the tire structure model in estimating tire radial behavior was examined by comparing the vertical force at the spindle and tire contact patch area from the model to those from the experimental results. Finally, tire longitudinal and lateral force test data from the FlatTrac machine were exploited in the developed optimization algorithm to estimate the tire model parameters in longitudinal and lateral directions.

Different case studies were simulated in order to analyze the performance of the developed model. For evaluating the dynamic behavior of the tire structure model, cleat test simulations were conducted, and model results were compared with three commercially available tire models. The HSSTM was able to negotiate a rectangular cleat (short wavelength road perturbation). The estimated tire vertical displacement, vertical load, and longitudinal force at the spindle were correlated with experimental data (Part II paper [2] presents more details on the experimental work conducted.)

For the validation case studies on deformable surfaces, driving and cornering maneuvers were conducted at constant normal load and varying slip values. Experimental tests were performed on the Terramechanics test rig at Virginia Tech using the Michelin LTX 235/85R16. The tests were performed on sandy loam, and data were collected for various case studies and parameter changes [12,13,14]. By means of the cross-plot validation graphs it was shown that the HSSTM can estimate three main vehicle handling parameters including longitudinal force, lateral force, and sinkage with a reasonable accuracy. Using a deformable tire structure model, the HSSTM produced more accurate contact patch pressure distributions and consequently more accurate sinkage and force estimations compared to the rigid wheel model (when simulated with NWVPM).

8. Acknowledgments

This work has been partially supported by the Cooperative Agreement W56HZV-14-2-0001 US Army TARDEC/ARC, by the European Union Horizon 2020 Framework Program, Marie Sklodowska-Curie grant agreement no. 645736, by the Terramechanics, Multibody, and Vehicle Systems (TMVS) Laboratory and the NSF I/UCRC Center for Tire Research (CenTiRe) at Virginia Tech, U.S.A., and by the Vehicle Dynamics Group at the University of Pretoria, South Africa.

9. References

1. Sandu, C., Taheri, Sh., Taheri, S., and Gorsich, D. – "*Hybrid Soft Soil Tire Model (HSSTM). Part I: Tire Material and Structure Modeling*", J. of Terramechanics, on-line August 10, 2019, Vol. 86, pp. 1-13 (13), https://doi.org/10.1016/j.jterra.2019.08.002, Dec. 2019.
2. Sandu, C., Taheri, Sh., Taheri, S., and Gorsich, D. – "*Hybrid Soft Soil Tire Model (HSSTM). Part II: Tire-Terrain Interaction*", J. of Terramechanics, on-line August 10, 2019, Vol. 86, pp. 15-29 (15), https://doi.org/10.1016/j.jterra.2019.08.004, Dec. 2019
3. Taheri, S., *Finite Element Modeling of Tire-Terrain Dynamic Interaction for Full Vehicle Simulation Application*, M.S. Thesis, 2014, Mechanical Engineering Department, Virginia Tech, Blacksburg, VA, USA.
4. Taheri, Sh., Sandu, C., and Taheri, S., *Finite Element Modeling of Tire Transient Characteristics in Dynamic Maneuvers.* SAE Int. J. Passeng. Cars - Mech. Syst., 2014. **7**(1): p. 221-230.
5. Taheri, S. and T. Wei, *A New Semi-Empirical Method for Estimating Tire Combined Slip Forces and Moments during Handling Maneuvers.* SAE International Journal of Passenger Cars-Mechanical Systems, 2015. **8**(2015-01-9112): p. 797-815.
6. Dennis Jr, J.E., Gay, D.M., and Walsh, R.E., *An adaptive nonlinear least-squares algorithm.* ACM Trans. on Mathematical Software (TOMS), 1981. **7**(3): p. 348-368.
7. Marquardt, D.W., *An algorithm for least-squares estimation of nonlinear parameters.* J. of the Society for Industrial & Applied Mathematics, 1963. **11**(2): p. 431-441.
8. Bellavia, S., Macconi, M., and Morini, B., *An affine scaling trust-region approach to bound-constrained nonlinear systems.* Applied Numerical Mathematics, 2003. **44**(3): p. 257-280.
9. Coleman, T.F. and Li, Y., *A reflective Newton method for minimizing a quadratic function subject to bounds on some of the variables.* SIAM J. on Optimization, 1996. **6**(4): p. 1040-1058.
10. Lugner, P. and Plöchl, M., *Tyre model performance test: First experiences and results.* Vehicle System Dynamics, 2005. **43**(sup1): p. 48-62.
11. Zegelaar, P.W.A., *The dynamic response of tyres to brake torque variations and road unevenesses*. 1998: TU Delft, Delft University of Technology.

12. Naranjo, S., Sandu, C., Taheri, S., Taheri, Sh., *Experimental Testing of an Off-Road Instrumented Tire on a Soft Soil*, J. of Terramechanics,2014, **56**: p. 119-137, doi:10.1016/j.jterra.2014.09.003.

13. Naranjo, S.D., "*Experimental Investigation of the Tractive Performance of an Instrumented Off-Road Tire on a Soft Soil Terrain*", M.S. Thesis, 2013, Mechanical Engineering Department, Viginia Tech, Blacksbutg, VA, USA.

14. Taheri, Sh., Sandu, C., and Taheri, S – "Development and Implementation of a Hybrid Soft Soil Tire Model (HSSTM)", Proc. of the 18th Int. Conf. of the ISTVS, Sept. 22-25, 2014, Seoul, Korea.

15. Wong, J.Y., *Theory of Ground Vehicles*. 4th ed. 2008, Hoboken, NJ: John Wiley & Sons.

16. Jimenez, E. and Sandu, C. – "Handling Performance of Pneumatic Tires on Sandy Loam", Paper no. 2015017, The 13th European Conf. of the ISTVS, Oct. 21-23, 2015, Rome, Italy.

17. Taheri, Sh. - "*A Hybrid Soft Soil Tire Model (HSSTM) for Vehicle Mobility and Deterministic Performance Analysis in Terramechanics Applications*", Ph.D. Dissertation, Mechanical Engineering Department, Blacksburg, VA, USA, Aug. 28, 2015,